Organic Electronics 13 (2012) 687–696

Contents lists available at SciVerse ScienceDirect

Organic Electronics

journal homepage: www.elsevier.com/locate/orgel

Effect of side groups on the vacuum thermal evaporation of polythiophenes for organic electronics

Peter Kovacik [a,*], Shawn M. Willis [a], Jonathan D. Matichak [b], Hazel E. Assender [a], Andrew A.R. Watt [a,*]

[a] Department of Materials, University of Oxford, Parks Road, OX1 3PH Oxford, United Kingdom
[b] Department of Chemistry, University of Oxford, 12 Mansfield Road, OX1 3TA Oxford, United Kingdom

ARTICLE INFO

Article history:
Received 20 October 2011
Received in revised form 13 January 2012
Accepted 13 January 2012
Available online 2 February 2012

Keywords:
Organic solar cells
Conjugated polymers
Poly(3-hexylthiophene)
Polythiophene
Vacuum thermal evaporation
Thin films

ABSTRACT

The vacuum thermal evaporation of poly(3-hexylthiophene) (P3HT) and poly(thiophene) (PTh) conductive polymers with and without side groups is reported. The role of side groups in relation to structural and electronic properties is examined. FT-IR and GPC analysis is used to study the effect deposition has on conjugation of the polymer. Topography and grain structure of the polymer films are studied using MicroXAM, AFM and TEM. XRD and TEM data reveal enhanced molecular packing and crystallinity of PTh. This results in significantly improved charge transport properties with relatively high hole mobilities (10^{-4} cm^2/Vs). Evaluation of PTh and P3HT electronic properties is performed on simple geometry planar C_{60} heterojunction solar cells. PTh/C_{60} devices exhibit almost a 70% increase in efficiency as compared to P3HT/C_{60} devices, demonstrating enhanced charge collection in PTh films through improved molecular order.

1. Introduction

Organic semiconductors for low-cost electronics, including photovoltaics, are attractive because they can be deposited cheaply via roll-to-roll processes using either solvents or vacuum evaporation [1,2]. Vacuum thin film deposition onto polymer substrates is an inexpensive and commonly used method widely exploited, for example, in the packaging industry [3–5]. Among its prevailing advantages are a complete absence of solvents, good control over the film thickness, and the parallel and sequential deposition of complex multilayer structures which are unmatched by solution processing. Polymer semiconductors are often chosen over their molecular and oligomeric counterparts due to their attractive properties in printing inks, and preferable response to morphological development during or after deposition [6,7]. Thus we sought to examine the vacuum deposition of polymeric semiconductors and demonstrate efficiencies comparable to solution deposited equivalents. We explore the influence side groups have on the chemical, physical and electronic properties of poly(thiophene) (PTh) and poly(3-hexylthiophene) (P3HT).

Polythiophenes form a family of conjugated polymers that has been investigated for more than three decades [8–10]. Their distinctive electronic properties have stimulated their application in many fields of electronics and optics, such as chemical and biological sensors, field-effect transistors, photovoltaic cells and light-emitting diodes [11–18]. Efficient charge transport in conjugated systems occurs via strong coupling of the polymer electronic states. Polymer structure determines both backbone planarity and π stacking which influences intra and inter-chain electronic processes [19–21]. Polymers with no side groups have the opportunity for enhanced backbone packing and electronic properties in the solid state [22,23], however for their effective processing in solution side groups have to be added.

* Corresponding authors. Tel.: +44 (0) 1865 613455.
E-mail addresses: peter.kovacik@materials.ox.ac.uk (P. Kovacik), andrew.watt@materials.ox.ac.uk (A.A.R. Watt).

1566-1199/$ - see front matter © 2012 Elsevier B.V. All rights reserved.
doi:10.1016/j.orgel.2012.01.005

Since the discovery of electrical conductivity in polythiophene, many attempts have been made to improve its solubility while preserving its unique properties. Introduction of alkyl groups onto the polythiophene backbone lead to a successful trade-off between solubility and conductivity [24]. Presence of these groups, however, results in distortions of the backbone conformation and thus various side effects, such as thermochromism or solvatochromism [25]. Layered structures have alkyl side groups acting as spacers between the backbone stacks thus allowing delocalisation of molecular orbitals in only two dimensions of the polymer crystal (separation within the backbone plane is shown in Fig. 1). In addition, high regioregularity of polythiophenes is required to prevent molecular disorder [26]. It has been shown that intermolecular packing is reduced by increased side-chain disorder with longer alkyl side groups in polythiophenes [27] and several studies of hole transport in thin films of poly(3-alkylthiophene)s have revealed a decrease in mobility as a function of increasing side-chain length [28–31]. These are just some of the examples, in which optical and electronic properties of the polymers are compromised by their need for solubility [28].

Various deposition methods have been explored to enhance the molecular order and packing in polythiophene thin films. These included Langmuir–Blodgett films [32,33], electrochemical polymerisation on conductive surfaces [34–36], or transformation of soluble precursor polymers [37–39]. Many of these techniques, however, lack scalability and throughput necessary for industrial application, while others involve reactions (e.g. heating, UV-light) which cause degradation of other device components or leave by-product residues. Standard solution coating and printing are thus the only widely investigated methods for large-scale processing of conjugated polymers [1,40].

Vacuum thermal evaporation of large organic molecules already has a long tradition [41,42] and has been successfully applied to various polymers, mostly Teflon and nylon in metal–polymer nanocomposite systems [43–48]. Although the main shortcoming is the decrease in molecular weight during the thermal heating, small polymers with up to several 1000s gmol^{-1} equivalent to 10s of monomeric units can be deposited [41] and therefore still possess their long-chain character. This macromolecular character might be beneficial in achieving controlled phase-separation in vacuum-deposited bulk heterojunctions.

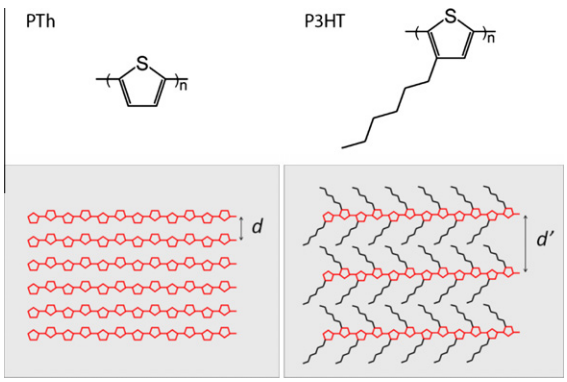

Fig. 1. Molecular structure of P3HT and PTh with a simple model of their molecular packing. PTh chains pack with closer proximity (d) than P3HT (d′) due to the lack of side groups.

In 2009, Wei et al. employed simple vacuum thermal evaporation to deposit thin films of P3HT [49] and showed that polymers can be thermally evaporated while retaining their chemical composition and structure. In 2011, our group confirmed this, and additionally demonstrated the fabrication of functional P3HT/C_{60} photovoltaic devices with efficiencies comparable to solvent deposited devices of the same architecture [50].

In this paper, we examine the thermal vacuum deposition of unsubstituted polythiophene and compare its structural and electronic properties with P3HT. We show that PTh molecules assemble into ordered films with high crystallinity, leading to enhanced charge transport properties. To illustrate the potential of polythiophene thin films in electronic and optoelectronic applications, PTh/C_{60} photovoltaic cells are fabricated and detailed characterisation performed.

2. Materials and methods

2.1. Materials

Poly(3-hexylthiophene) (P3HT) was purchased from Rieke Metals. The molecular weight (M_w) was measured using gel permeation chromatography (GPC) and was found previously to be $M_w = 36257$ gmol^{-1} with respect to polystyrene standards. The regioregularity of the polymer was reported by the manufacturer to be 90%. Poly(thiophene) (PTh) was supplied by Sigma Aldrich and its M_w was not measured as it did not dissolve in tetrahydrofuran, the mobile phase of GPC. Poly(3,4-ethylenedioxythiophene)-poly(styrenesulfonate) (PEDOT:PSS, Baytron P dispersion) was supplied by H.C. Starck. Fullerene C_{60} (99.9% pure) was purchased from MER Corporation. All the materials were used as received.

2.2. Polymer deposition

Polymers (PTh, P3HT) were deposited by thermal evaporation from a tungsten boat (Leybold Optics) which was heated by a Xantrex XHR 7.5-80 DC Power Supply. The evaporation was conducted in high vacuum $\sim 1 \times 10^{-5}$ Torr. The boat temperature was measured using a K-type exposed thermocouple mounted inside the boat. For chemical characterisation, PTh was deposited at a temperature of 275 ± 5 and 300 ± 5 °C at a rate of ~1 nm/min. For photovoltaic device fabrication, PTh was deposited at a temperature of 300 ± 10 °C and P3HT at 415 ± 10 °C, both at a rate of ~1 nm/min. Since our previous study [50] we have found that higher temperatures of P3HT deposition lead to improved device performance.

2.3. Chemical characterisation

Thermal analysis of starting PTh was measured by DSC (Perkin Elmer Diamond DSC) between −60 and 225 °C at rates of 100 and 300 °C/min, and by TG/DTA (Perkin Elmer

Pyris Diamond TG/DTA 6300) under N_2 atmosphere between 25 and 800 °C at a rate of 10 °C/min. Following the vacuum deposition of PTh onto a series of cleaned glass-slides, the polymer films were dissolved in chloroform. However, the starting PTh could only be partially dissolved in chloroform. The solutions were characterised by UV–Vis-NIR spectroscopy (Agilent Cary 5000) and infrared spectroscopy (Varian UMA-600). Infrared spectra of PTh were measured with an attenuated total reflectance extension on the FT-IR spectrometer (the solution being cast onto the crystal window). GPC was carried out using PLgel 5 μm Mixed-D columns (2 × 300 mm length, 7.5 mm diameter) from Polymer Laboratories. The calibration was performed using polystyrene narrow standards ($Mp = 580–3.7 \times 10^5\ gmol^{-1}$) in tetrahydrofuran (THF) with toluene as the flow marker, detecting at 254 nm. The THF was degassed with helium and pumped at a rate of 1 mL/min at 40 °C. Since most of the materials characterization was necessarily performed in air, the exposure to air, light and moisture was minimised to limit any effect of oxidation that may have been introduced.

2.4. Polymer film characterisation

The surface morphology of the thin films was imaged by MircoXAM surface mapping microscope (ADE Phase Shift) and atomic force microscope (AFM) data was collected using an AutoProbe CP (Park Scientific Instruments) in tapping mode. X-ray diffractometry was performed on a Philips PW1820 system with PW1727 X-ray generator using Cu $K\alpha$ radiation ($\lambda = 1.5418$ Å). Polymer films were deposited on silicon wafer substrates by the process described above. The evaporation temperatures were the same ones as for device fabrication. The film thickness was approximately 0.3 μm for both PTh and P3HT (thicker PTh film in the inset of Fig. 6b was ~1 μm).

2.5. HRTEM analysis

HRTEM analysis was performed on a JEOL-JEM 4000EX LaB6 microscope with an information limit of 0.12 nm at an accelerating voltage of 100 kV and calibrated using lead sulphide nanocrystals with well-defined lattice spacings. Samples were prepared by taking a polymer film deposited on PEDOT and placing it in deionized water for 24 h, the PEDOT is dissolved and the polythiophene film floats off and is mounted on 400 mesh copper TEM grid.

2.6. Device fabrication

Photovoltaic devices were prepared by sequentially thermally evaporating PTh (or P3HT) and C_{60} in between an Al cathode and an ITO-on-glass anode as follows. The ITO surface was cleaned with acetone and isopropanol and then treated with oxygen plasma for 5 min. A layer of PEDOT:PSS was spin coated at 5000 rpm for 30 s onto the prepared ITO surface and then heated for 5 min at 140 °C. Next, a layer of PTh (or P3HT) and a layer of C_{60} were sequentially deposited onto the substrate by vacuum thermal evaporation. The layer thickness was controlled *in situ* using a quartz crystal microbalance (Q-Pod, Inficon) placed at the same distance from the source as the substrates. After the deposition, the value was further verified by Veeco DEKTAK surface profiler (Dektak 6 M Stylus Profiler). Finally, a set of 80 nm thick Al electrodes was evaporated on top of the sandwich structure. The active device area was 2.2 mm^2.

Hole-only devices for carrier mobility and lifetime measurements were fabricated as described above, excluding the C_{60} deposition step. The thickness of the PTh films was 130 nm. As reported previously [50], P3HT does not adhere well to annealed PEDOT:PSS surface and therefore various modifications of the surface were investigated (ITO, plasma-treated ITO, plasma-treated PEDOT:PSS, non-annealed PEDOT:PSS). The best results were obtained for PEDOT:PSS plasma-treated for 2 min. Although dewetting phenomenon was observed here as well, the thickness of the continuous part of the film was estimated to be around 65 nm.

2.7. Electronic characterisation

Photovoltaic characterisation of the devices was carried out under white light illumination (AM1.5, 100 mW/cm^2) in an inert N_2 atmosphere. The light intensity at the sample position was determined with a microprocessor-based power meter (Thermo-Oriel Instruments, Model No. 70260) calibrated according to ASTM standards. A set of neutral ND filters (Melles Griot) were used for varying the illumination intensity. Current–voltage characteristics were measured using a Keithley 2400 source measurement unit. Impedance measurements were performed with an Agilent E4980A opt001 LCR meter at biases from 0 to 3.0 V in the frequency range of 20 Hz–2 MHz. Each measurement was taken in the R-X mode and the AC signal was set to 25 mV. All impedance measurements were performed in the dark. The purpose-built chamber provided electrical shielding.

3. Results and discussion

3.1. Chemical characterisation

Prior to thin film deposition, the thermal stability of PTh was studied by thermogravimetric analysis (TGA) under an N_2 atmosphere at atmospheric pressure. The onset of polymer degradation under nitrogen (note, not the vacuum condition of the deposition) was identified at approximately 272 °C with weight loss of 5 wt.% at 300 °C. This is in good agreement with the findings reported previously by Mo et al. [51]. Thermal behaviour of the polymer was analysed by differential scanning calorimetry (DSC) and differential thermal analysis (DTA), however, no evident phase-transition peaks were found. Similar thermal behaviour has been observed also by other groups [52,53]. The absence of an apparent glass-transition suggests a high level of crystallinity in the starting material.

Thin films of PTh were deposited by evaporating it at 275 and 300 °C at a vacuum base pressure of 10^{-5} Torr. Two different temperatures were chosen to determine the influence of heating on the chemical structure of the

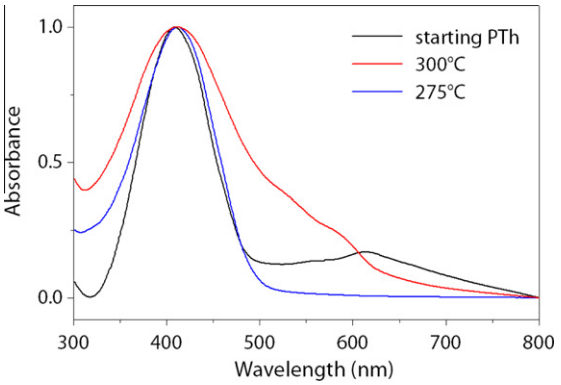

Fig. 2. UV–Vis absorption spectra of PTh evaporated at 275 and 300 °C in comparison with the starting material. The absorption peaks are normalized to the highest intensity.

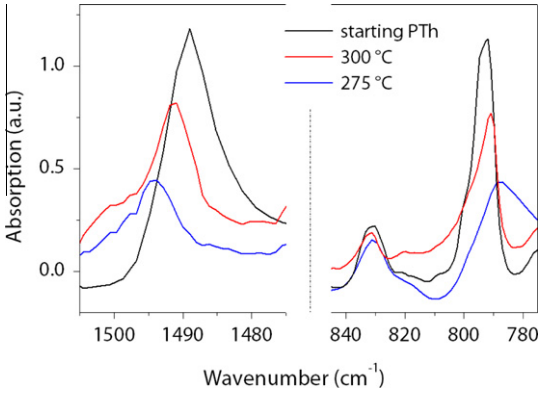

Fig. 3. Bands of FT-IR spectra related to conjugation length of starting PTh and PTh after evaporation at 275 and 300 °C.

polymer. At 275 °C, the onset of a measurable evaporation rate was detected at this pressure, and 300 °C was the temperature at which only a minor weight loss (≈5%) was measured by TGA under nitrogen. Similar temperatures (300–310 °C) under N_2 atmosphere and atmospheric pressure have commonly been used for conversion of precursor polymers into unsubstituted polythiophene in solution-processed heterojunction solar cells [23,38]. Fig. 2 shows UV–Vis spectra of chloroform solutions of the evaporated PTh and the starting material. The three curves are normalized to their maximum intensity. The position of the absorption maximum of PTh at 408 nm (corresponding to the intramolecular π–π transition) remains almost unchanged by the evaporation process. Wider but symmetric peaks of the evaporated samples imply that the range of conjugation lengths is increased as a result of evaporation. The starting PTh has a shoulder peak at 614 nm, which likely comes either from an intermolecular π–π stacking and shows a presence of agglomerates [21,54]. The peak is shifted towards smaller wavelengths for PTh evaporated at 300 °C and disappears completely for the polymer evaporated at 275 °C. This suggests that the higher temperature process gives rise to greater crystal packing and agglomeration.

For evaporated PTh (300 °C), the thin film absorption spectrum is considerably more red-shifted in respect to the chloroform solution (7 nm) than it is in the case of P3HT (a blue shift of 2 nm, see Supplementary information). Moreover, the band broadening is more significant in the PTh film compared to P3HT. Thus we can conclude, that PTh molecules have better aggregation and stacking in solid films than those of P3HT. The XRD data (shown later, in Fig. 6) indicate that the crystallinity of evaporated PTh is greater than in evaporated P3HT films.

Structural NMR and FT-IR studies of P3HT have previously shown that the polymer conjugation length decreases during the evaporation and side groups dissociate from the backbone [50]. Due to the absence of side groups in PTh, a decrease in conjugation length was expected to be the only major structural change caused by thermal heating. FT-IR spectroscopy was used to study changes in conjugation, as shown in the Fig. 3 (for detailed analysis of the full spectra, see Supplementary information). As the ratio of symmetric (1439 cm^{-1}) to asymmetric (1489 cm^{-1}) C=C stretching vibrations refers to the conjugation length of polythiophene [55], all three spectra were normalized to the intensity of the 1439 cm^{-1} peak in order to directly compare the degree of conjugation. Table 1 summarizes changes in positions and intensities of the peaks.

The band 780–840 cm^{-1} (related to the thiophene ring vibrations) shows a shift and increase of the 787 cm^{-1} peak, indicating decrease in conjugation length of the polymer [56]. Similar trends can be seen in the range 1480–1500 cm^{-1}, where the 1489 cm^{-1} peak (normalized against 1439 cm^{-1}) decreases and consistently shifts to 1491 and 1494 cm^{-1} for 300 and 275 °C, respectively. Both these changes imply loss in the polymer conjugation [55,57]. Interestingly, the higher evaporation temperature (300 °C) leads to a higher molecular weight being deposited. Since the processing temperature is around the vaporization temperature, bigger molecules can be evaporated at the higher temperature.

Using gel permeation chromatography (GPC), we have already shown that the molecular weight of P3HT is reduced following thermal evaporation from ~36,000 $gmol^{-1}$ to ~1500 $gmol^{-1}$, equivalent to a degree of polymerization of about nine [50]. GPC of evaporated and starting PTh was limited by poor solubility in tetrahydrofuran the mobile phase of the GPC. The starting material could not be dissolved at all while only a small percentage of the evaporated

Table 1
Main band assignments and intensity changes in the FTIR spectra of PTh.

Wavenumber	Vibration	On evaporation
787	Thiophene ring vibration [56]	Shifted and increased
831	Terminal thiophene ring vibration [56]	Similar
1439	Symmetric C=C stretching vibration [55]	Normalization peak
1489	Asymmetric C=C stretching vibration [55]	Shifted and decreased

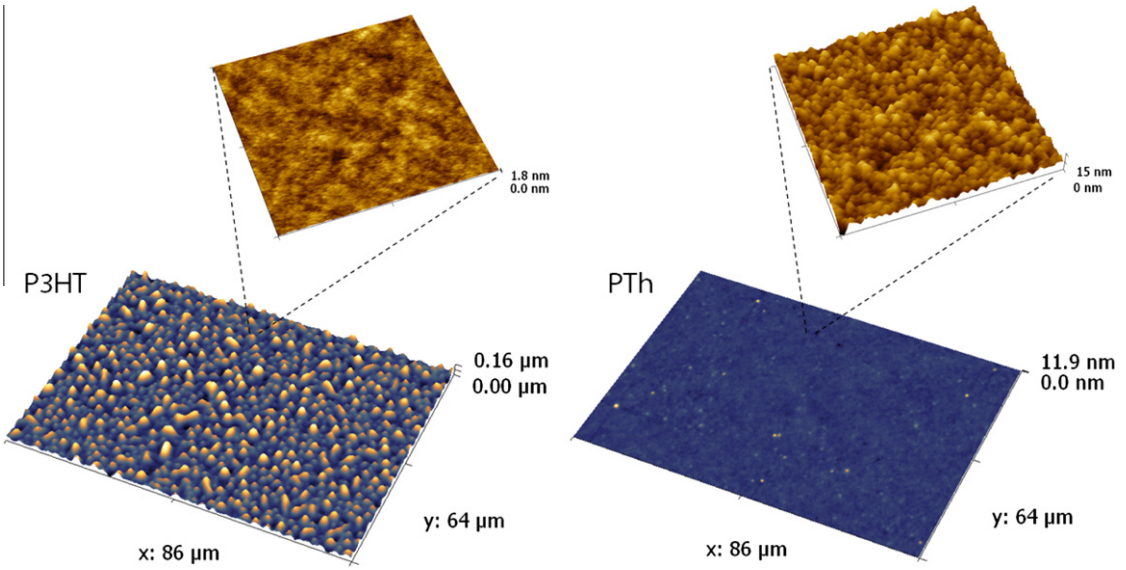

Fig. 4. MicroXAM images of 70 nm thick P3HT (left blue) and PTh (right blue) films on PEDOT:PSS coated ITO substrate. Scaled insets (brown) are high resolution 1 × 1 µm AFM scans (positions of the scaled areas are only illustrative). (For interpretation of the references to colour in this figure legend, the reader is referred to the web version of this article.)

Table 2
RMS roughness values for MicroXAM and AFM scans of P3HT and PTh films.

	P3HT (86 × 64 µm)	PTh (86 × 64 µm)	P3HT (1 × 1 µm)	PTh (1 × 1 µm)
RMS roughness (nm)	26.10	0.35	0.21	1.77

sample could. The evaporated PTh that was dissolved had a $M_w \approx 900$–$1000\ \mathrm{gmol}^{-1}$ corresponding to a degree of polymerization of about 11–12. We believe that the overall average molecular weight of the evaporated material to be much higher once the insoluble component is included.

3.2. Morphological characterisation

Following the chemical characterisation of PTh, polymer thin films were deposited directly onto a PEDOT:PSS electrode surface and their topography (Fig. 4) and roughness (Table 2) studied at both macro- and nano-scale. Fig. 4 shows a comparison of the surface profile of P3HT (a) and PTh (b) layers measured by MicroXAM optical profiler. P3HT film dewets the PEDOT:PSS and forms island-type structures. As shown previously [50], such poor substrate wetting causes large variations in the film thickness leading to low shunt resistance of the active layer due to partial shorting across the device. In contrast, PTh coats the surface and creates a microscopically flat film.

Higher resolution topography of the layers was obtained from AFM scans (scaled insets of Fig. 4). At this scale P3HT films are relatively smooth, while the PTh is composed of grains between 20 and 50 nm in diameter. The featureless character of the former might result from packing disorder caused by side group dissociation, and the appearance of grains in the latter might be consistent with packing of the PTh molecules into more ordered agglomerates. The difference in roughness accounts for less than ~5% of the overall surface area and so is not making a large difference to the area for charge separation in devices. The low magnification bright TEM image shown in Fig. 5a suggests a slightly smaller grain size of between 5 and 20 nm. High resolution phase contrast imaging (Fig. 5b) of these grains shows that they are made of single crystals of polythiophene. A diffraction pattern (Fig. 5c) shows that these crystal grains are orientated in different directions and that

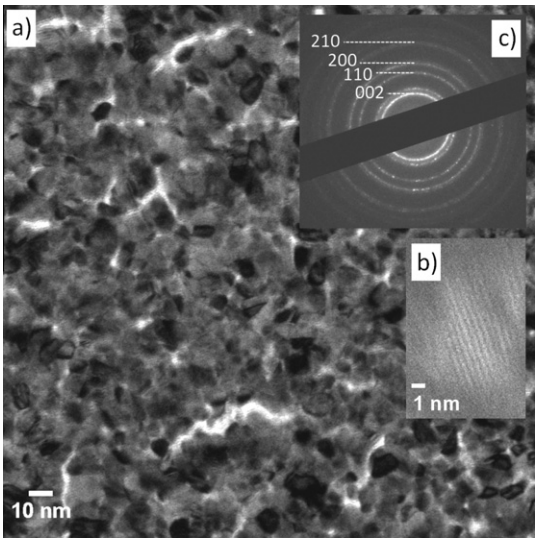

Fig. 5. (a) Bright TEM image of PTh grains. (b) Phase contrast image of a single polythiophene crystal. (c) Diffraction pattern of PTh with crystallographic planes indexed.

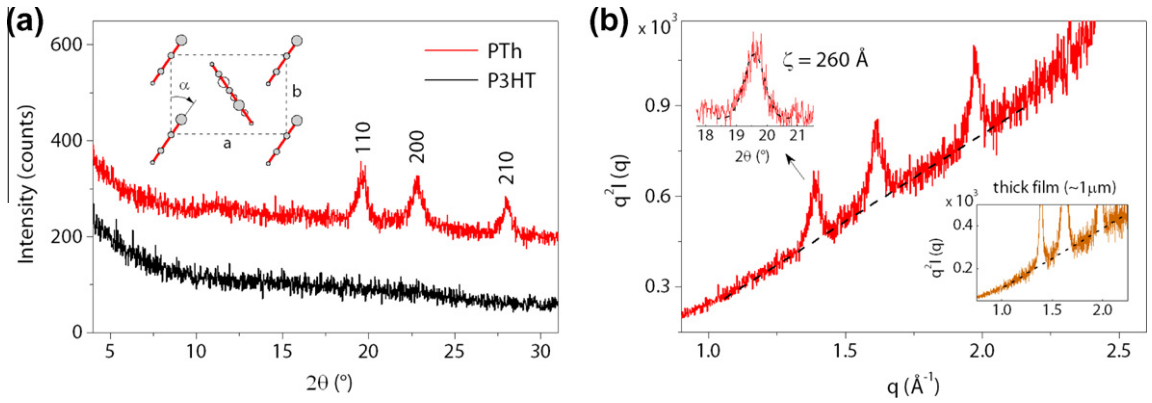

Fig. 6. (a) XRD traces of PTh and P3HT deposited on silicon wafers. Inset of the figure shows unit cell of PTh with the herringbone packing motif. (b) XRD intensity curve $q^2I(q)$ of PTh with Gaussian fit of the peak 110 (upper inset) and intensity curve of 1 μm thick PTh film (lower inset).

the plane spacing corresponds with other TEM and XRD studies [51,58]. TEM of the P3HT samples shows an amorphous structure with no grains or crystal structure present and an amorphous diffraction pattern.

XRD patterns of the PTh film taken normal to its plane suggest substantially higher crystallinity in PTh than its P3HT counterpart (Fig. 6). Such θ–2θ XRD analysis does not map the full range of crystal orientations, and so the intensities do depend on the orientational distribution of the crystals. Diffraction peaks at 19.6°, 22.8° and 28.0° are in agreement with literature data and correspond to 110, 200 and 210 reflections of polythiophene [51,59]. The (hk0) indexing of reflections suggests polythiophene chains lie in the plane of the substrate [59]. The calculated lattice parameters are a = 7.80 Å, b = 5.51 Å and $c \approx 7.70$ Å (estimated from the thiophene monomer [60]), all consistent with either a monoclinic or orthorhombic unit cell with the molecules rotated around their axis by alternately $\alpha \approx \pm 31°$ to the unit cell b axis [51,60]. This rotation leads to a standard herringbone packing motif as shown in the inset of Fig. 6a. Precise parameters as well as determination of monoclinic angle β would require analysis of a more detailed data set.

The degree of crystallinity, X_{cr}, of a polymer can be estimated as the ratio between the intensity of the diffraction peaks over the total diffracted intensity (including amorphous areas). The values of X_{cr} = 35–40% have been found for unannealed polythiophene powder [51,59]. In order to analyse the contribution of the amorphous background, the data of Fig. 6a were replotted as $q^2I(q)$ vs. q (Fig. 6b), where $q = 4\pi(\sin\theta)/\lambda$ is the magnitude of the scattering vector and $I(q)$ is the total scattered intensity. This allowed us to resolve the total intensity into the background diffuse scattering and the crystalline diffraction. As seen from the plot, the baseline of the diffraction peaks appears linear (fitted by the dotted line) with no signs of amorphous phase present in this orientation. Similar results were obtained from the analysis of thick-film samples (≈1 μm, see lower inset of Fig. 6b), neither was any amorphous background found outside the plotted range. In accordance with results of the previous studies [51,59], this implies that the PTh films have very high crystallinity after the vacuum deposition.

Additionally, a coherence length ξ = 260 Å of the polymer was calculated from Debye–Sherrer relation [61].

$$\xi = 57.3\lambda/(\beta\cos\theta) \quad (1)$$

where $\beta = (B^2 - b_0^2)^{1/2}$, B is the measured half-width of the peak (in degrees), b_0 is the instrumental resolution (<0.05°), λ is the wavelength of the X-radiation (1.5418 Å), 2θ is the scattering angle. Half-width B was obtained from Gaussian fit of the peak 1 1 0, as seen in upper inset of Fig. 6b.

3.3. Electronic characterisation

A high degree of molecular orientation and crystallinity of polymers can improve the charge carrier transport. The space charge limited current (SCLC) technique was therefore used to measure hole mobility μ_0 of the PTh and P3HT films. Hole-only devices were fabricated by depositing a polymer layer between ITO bottom and a hole-injecting gold top electrode (due to the limited wetting of the surface by P3HT, modification of the PEDOT:PSS was necessary; for more details see Section 2). Fig. 7 shows the current density as a function of the applied voltage (corrected for the built-in voltage $V_{BI\ PTh} \approx 0.05$ V, $V_{BI\ P3HT} \approx 0.02$ V). While the slope of the curves at low voltages is equal to 1 (see log–log Fig. 7a) and reflects linear Ohmic behaviour of the devices, the slope at higher voltages is 2, indicating the presence of space charge limited current.

In this regime, the electrode injects more holes than the material can transport and the J–V dependence become quadratic as quantitatively described by the Child's law [62].

$$J = \frac{9}{8}\varepsilon_0\varepsilon_r\mu_0\frac{V^2}{L^3} \quad (2)$$

where ε_0 is permitivity of free space, ε_r is the dielectric constant, μ_0 is the mobility, V is potential and L is the film thickness (in our case 130 nm for PTh and 65 nm for P3HT). The equation fitted to the experimental data leads to the hole mobilities $\mu_{0\ PTh} = 2.03 \times 10^{-4}$ cm^2/Vs and $\mu_{0\ P3HT} = 1.05 \times 10^{-6}$ cm^2/Vs (Fig. 7b). While the value for P3HT

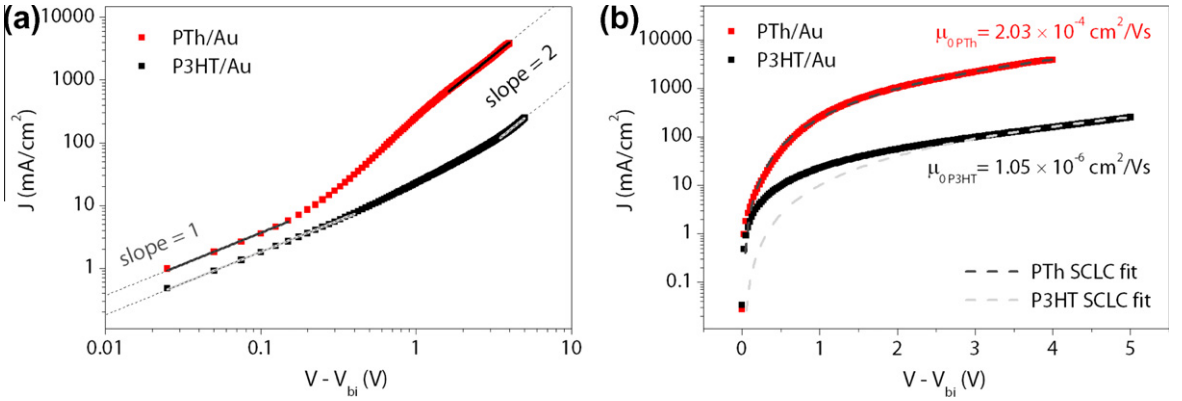

Fig. 7. (a) Dark *J–V* characteristics of an ITO/PEDOT:PSS/polymer/Au devices in double-logarithmic scale. Fitted are low-voltage region with Ohmic character (slope = 1) and space charge limited region above >1 V (slope = 2). (b) The same *J–V* characteristics in semi-logarithmic scale fitted by single-carrier SCLC (Child's law).

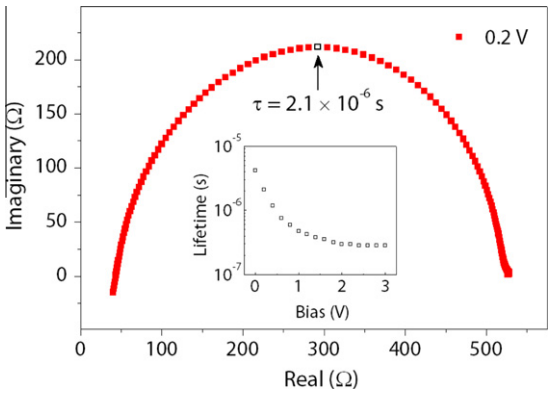

Fig. 8. The characteristic frequency of a PTh device with a gold electrode for 0.2 V forward bias. The inset displays the carrier lifetime as a function of forward bias.

appears very low, for PTh it is comparable with the best photodiode mobilities achieved for ordered high molecular weight P3HT deposited from solution [62,63].

A minority carrier lifetime τ for PTh was calculated from the characteristic peak angular frequency, ω, in the impedance spectrum (Fig. 8) through the relation [64].

$$\omega = \tau^{-1}. \tag{3}$$

The resulting value is $\tau = 2.1 \times 10^{-6}$ s for 0.2 V forward bias, decreasing as the bias increases (as shown in the inset of Fig. 8). The short time scale 10^{-3}–10^{-4} ms implies high losses caused by electron–hole bimolecular recombination along the absorber layer or at the contact surfaces [64].

3.4. Photovoltaic devices

The optoelectronic behaviour of PTh films was studied in a planar heterojunction solar cell configuration ITO/PEDOT:PSS/polymer/C_{60}/Al in order to directly compare the effect of the materials properties without the greater variability in morphology associated with bulk heterojunctions or annealing [65–68]. For comparison, P3HT-based cells were fabricated to determine the effect of side groups in vacuum-deposited devices. Initially, the optimal C_{60} layer thickness for constant PTh and P3HT was determined to be 50 nm for both. Following this, the polymer thickness was varied to optimise the overall device performance. Fig. 9 plots the main figures of merit (PCE, J_{sc}, V_{oc}, FF) as functions of the donor thickness while the best cell parameters are summarised in Table 3.

For P3HT/C_{60} devices, the best power conversion efficiency PCE = 0.30% was achieved with 8 nm-thick P3HT. The value compares favourably to that of spin-coated P3HT/C_{60} planar heterojunctions reported previously (PCE = 0.17% [69]). The trend of increasing J_{sc} with decreasing layer thickness suggests that the polymer thickness probably approaches the value of the exciton diffusion length [70] and thus the charge extraction improves. However, the poorly wetting thin P3HT layers (around 10 nm) are already subject to low shunt resistance and therefore decrease in V_{oc} [50].

PTh planar heterojunctions exhibited significantly better performance. Optimal donor thickness was found to be 44 nm, leading to PCE = 0.52% (current–voltage behaviour of the optimised PTh and P3HT devices is shown in Fig. 10a and their absorption in Fig. 10b). The *J–V* curves indicate that the large, almost 70% increase in efficiency results from enhanced charge collection in PTh films through improved current parameters $J_{sc\ PTh} = 2.7$ mA cm^{-2} and $FF_{PTh} = 42.7$ (compared to $J_{sc\ P3HT} = 1.3$ mA cm^{-2}, $FF_{P3HT} = 32.9$). Noticeably, the higher photocurrent and the lower rate of recombination are directly affected by the molecular order and hole mobilities. This is also a result of better structural stability of PTh as opposed to P3HT, where dissociation of side groups can play various inhibition roles in charge transport. Open circuit voltage $V_{oc} = 0.45$ V of the PTh/C_{60} combination is defined by the position of the PTh HOMO level ($E_{HOMO} = 5.0$ eV [71]) and as such can be tailored by better molecular design.

The shape of the dark curves (inset of Fig. 10a) illustrates the difference in the quality of the donor/acceptor interfaces. While in case of P3HT/C_{60} only a poor rectification is observed, the interface of PTh/C_{60} displays much better diode characteristics. This is reflected also in the lower diode ideality factor $n_{PTh} = 2.6$ of the device

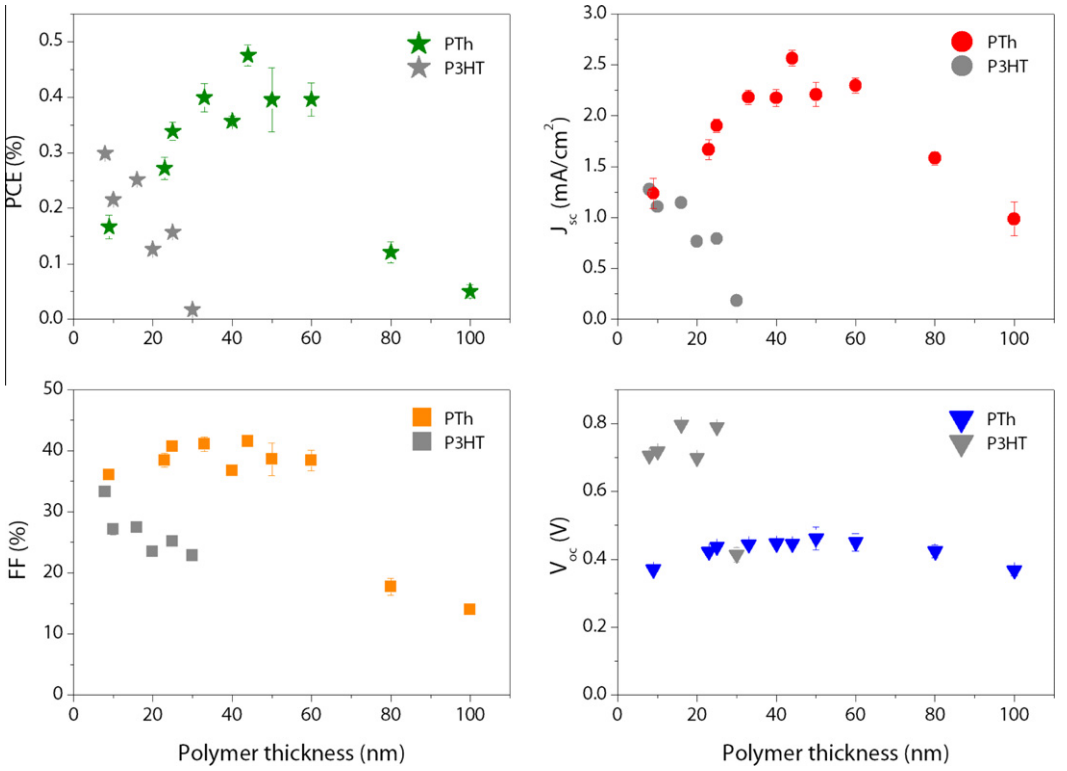

Fig. 9. Main figures of merit (PCE, J_{sc}, V_{oc}, FF) as functions of the polymer thickness for ITO/PEDOT:PSS/polymer/Al devices. Thickness of the C_{60} layer was constant 50 nm.

Table 3
Comparison of the PTh- and P3HT-based device parameters.

Device	Thickness (nm)	J_{sc} (mA/cm^2)	V_{oc} (V)	FF (%)	n	R_s (Ω cm^2)	μ_0 (cm^2/Vs)	PCE (%)
PTh/C_{60}	44	−2.70	0.45	42.7	2.59	25	2.03×10^{-4}	0.52
P3HT/C_{60}	8	−1.30	0.71	32.9	4.54	119	1.05×10^{-6}	0.30

(compared to $n_{P3HT} \approx 4.5$, see Table 3). The values of n and R_s were calculated from co-content function fit to the 4th-quadrant data section of the illuminated J–V curve.

As expected from the different molecular ordering in PTh and P3HT films, the series resistance of the polythiophene devices, $R_{s\ PTh} = 25\ \Omega\ cm^2$, was considerably lower than $R_{s\ P3HT} = 119\ \Omega\ cm^2$ despite having almost four times higher thickness.

Next, the effect of illumination intensity on the PTh/C_{60} device performance was measured (as shown in Fig. 11).

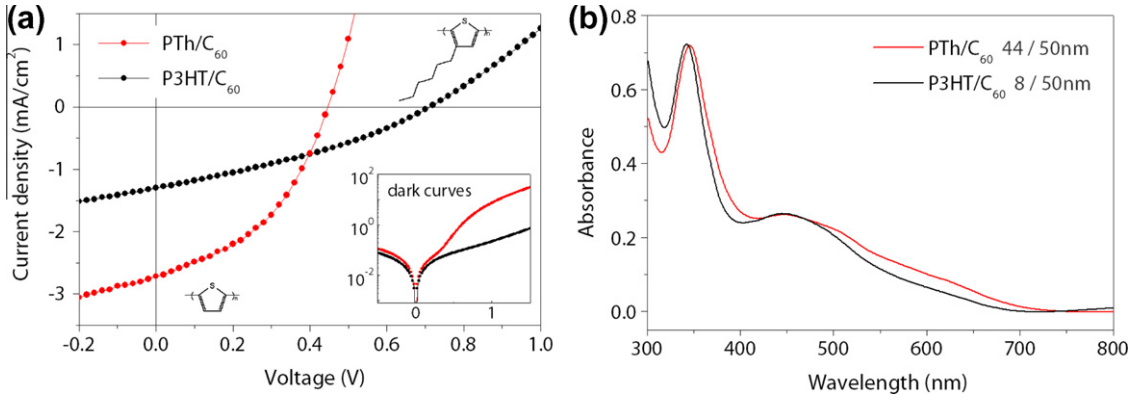

Fig. 10. (a) Comparison of J–V characteristics of the best performing PTh/C_{60} and P3HT/C_{60} devices. (b) UV–Vis absorbance spectra of the devices.

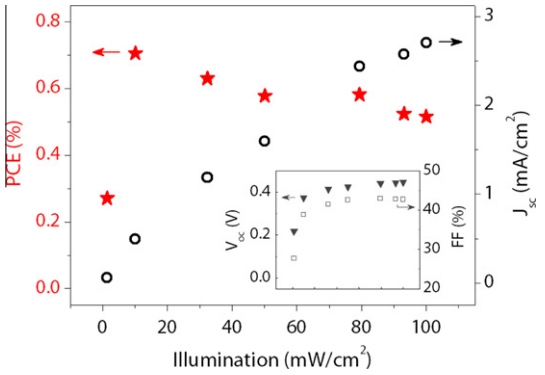

Fig. 11. J_{sc} (circles) and PCE (stars) of the PTh/C_{60} 44/50 nm cell as a function of incident illumination intensity. V_{oc} (triangles) and FF (squares) dependence is shown in the inset.

Although V_{oc} and FF remained relatively unchanged with decreasing illumination, J_{sc} increased nonlinearly causing PCE to increase. At 10 mW/cm^2, the PCE of the cell reached 0.71%. Similar behaviour has previously been observed for P3HT-based devices [50].

Enhanced performance of the PTh/C_{60} devices exceeded all untreated polythiophene and poly(alkyl-thiophene)/C_{60} planar heterojunctions reported so far [69,72] and is even comparable to bulk heterojunctions of un-substituted polythiophene and PCBM processed in solution [23]. Limited absorption and charge extraction of the PTh films may further be improved by post-production thermal annealing or by employing more complex solar cell designs, for instance multi-junction and bulk heterojunction architectures. These structures are currently under development.

4. Conclusion

This study has shown that polymer side groups have a strong influence on molecular packing and charge transport in vacuum-deposited polymer thin films. TEM and XRD data revealed, that unlike P3HT, evaporated PTh forms highly crystalline films without requiring annealing. The effect of molecular order was demonstrated on ITO/PEDOT:PSS/polymer/C_{60}/Al planar heterojunction solar cells. PTh-based devices had significantly better current (J_{sc}) and recombination (FF) characteristics, resulting in improved overall PCE by 70% as compared to P3HT.

We have successfully demonstrated that vacuum thermal evaporation is suitable for the deposition of low solubility polymers. The deposition method is compatible with current manufacturing processes and has good potential for low-cost production of highly ordered polymer thin films relevant to a plethora of electronic and optoelectronic applications.

Acknowledgements

The authors are grateful to Mr. Richard Turner for assistance with the TGA measurements, and to EPSRC and John Fell Fund for financial support.

Appendix A. Supplementary data

Supplementary data associated with this article can be found, in the online version, at doi:10.1016/j.orgel.2012.01.005.

References

[1] F.C. Krebs, Solar Energy Materials and Solar Cells 93 (4) (2009) 394.
[2] S.R. Forrest, Nature 428 (6986) (2004) 911.
[3] C. Bishop, Roll-to-Roll Vacuum Deposition of Barrier Coatings, Wiley-Scrivener, 2010.
[4] C. Bishop, Vacuum Deposition Onto Webs, Films and Foils, William Andrew, 2007.
[5] A.L. Roes, E.A. Alsema, K. Blok, M.K. Patel, Progress in Photovoltaics 17 (6) (2009) 372.
[6] S. Gunes, H. Neugebauer, N.S. Sariciftci, Chemical Reviews 107 (4) (2007) 1324.
[7] C.J. Brabec, S. Gowrisanker, J.J.M. Halls, D. Laird, S.J. Jia, S.P. Williams, Advanced Materials 22 (34) (2010) 3839.
[8] J.L. Bredas, B. Themans, J.G. Fripiat, J.M. Andre, R.R. Chance, Physical Review B 29 (12) (1984) 6761.
[9] T.A. Chen, X.M. Wu, R.D. Rieke, Journal of the American Chemical Society 117 (1) (1995) 233.
[10] X.W. Zhan, D.B. Zhu, Polymer Chemistry 1 (4) (2010) 409.
[11] H.A. Ho, M. Boissinot, M.G. Bergeron, G. Corbeil, K. Dore, D. Boudreau, M. Leclerc, Angewandte Chemie-International Edition 41 (9) (2002) 1548.
[12] L. Torsi, A. Dodabalapur, L. Sabbatini, P.G. Zambonin, Sensors and Actuators B-Chemical 67 (3) (2000) 312.
[13] H. Sirringhaus, P.J. Brown, R.H. Friend, M.M. Nielsen, K. Bechgaard, B.M.W. Langeveld-Voss, A.J.H. Spiering, R.A.J. Janssen, E.W. Meijer, P. Herwig, D.M. de Leeuw, Nature 401 (6754) (1999) 685.
[14] H. Sirringhaus, Advanced Materials 17 (20) (2005) 2411.
[15] S.H. Park, A. Roy, S. Beaupre, S. Cho, N. Coates, J.S. Moon, D. Moses, M. Leclerc, K. Lee, A.J. Heeger, Nature Photonics 3 (5) (2009) 297.
[16] G. Dennler, M.C. Scharber, C.J. Brabec, Advanced Materials 21 (13) (2009) 1323.
[17] A. Kraft, A.C. Grimsdale, A.B. Holmes, Angewandte Chemie-International Edition 37 (4) (1998) 402.
[18] I.F. Perepichka, D.F. Perepichka, H. Meng, F. Wudl, Advanced Materials 17 (19) (2005) 2281.
[19] T. Yamamoto, D. Komarudin, M. Arai, B.L. Lee, H. Suganuma, N. Asakawa, Y. Inoue, K. Kubota, S. Sasaki, T. Fukuda, H. Matsuda, Journal of the American Chemical Society 120 (9) (1998) 2047.
[20] R.D. McCullough, Advanced Materials 10 (2) (1998) 93.
[21] P.J. Brown, D.S. Thomas, A. Kohler, J.S. Wilson, J.S. Kim, C.M. Ramsdale, H. Sirringhaus, R.H. Friend, Physical Review B 67 (6) (2003).
[22] Y.D. Park, D.H. Kim, Y. Jang, J.H. Cho, M. Hwang, H.S. Lee, J.A. Lim, K. Cho, Organic Electronics 7 (6) (2006) 514.
[23] S.A. Gevorgyan, F.C. Krebs, Chemistry of Materials 20 (13) (2008) 4386.
[24] K.Y. Jen, G.G. Miller, R.L. Elsenbaumer, Journal of the Chemical Society-Chemical Communications 17 (1986) 1346.
[25] O. Inganas, W.R. Salaneck, J.E. Osterholm, J. Laakso, Synthetic Metals 22 (4) (1988) 395.
[26] Y. Kim, S. Cook, S.M. Tuladhar, S.A. Choulis, J. Nelson, J.R. Durrant, D.D.C. Bradley, M. Giles, I. Mcculloch, C.S. Ha, M. Ree, Nature Materials 5 (3) (2006) 197.
[27] T.J. Prosa, M.J. Winokur, J. Moulton, P. Smith, A.J. Heeger, Macromolecules 25 (17) (1992) 4364.
[28] A. Gadisa, W.D. Oosterbaan, K. Vandewal, J.C. Bolsee, S. Bertho, J. D'Haen, L. Lutsen, D. Vanderzande, J.V. Manca, Advanced Functional Materials 19 (20) (2009) 3300.
[29] K. Cho, Y.D. Park, D.H. Kim, Y. Jang, J.H. Cho, M. Hwang, H.S. Lee, J.A. Lim, Organic Electronics 7 (6) (2006) 514.
[30] K. Kaneto, W.Y. Lim, W. Takashima, T. Endo, M. Rikukawa, Japanese Journal of Applied Physics Part 2-Letters 39 (8B) (2000) L872.
[31] S.A. Chen, C.S. Liao, Macromolecules 26 (11) (1993) 2810.
[32] H. Nakahara, J. Nakayama, M. Hoshino, K. Fukuda, Thin Solid Films 160 (1–2) (1988) 87.
[33] T. Bjornholm, T. Hassenkam, N. Reitzel, Journal of Materials Chemistry 9 (9) (1999) 1975.
[34] R. Valaski, C.D. Canestraro, L. Micaroni, R.M.Q. Mello, L.S. Roman, Solar Energy Materials and Solar Cells 91 (8) (2007) 684.

[35] J.W. Yu, S.Y. Kim, K.H. Lee, B.D. Chin, Solar Energy Materials and Solar Cells 93 (1) (2009) 129.
[36] R. Advincula, C.D. Grande, M.C. Tria, G.Q. Jiang, R. Ponnapati, Macromolecules 44 (4) (2011) 966.
[37] J.S. Liu, E.N. Kadnikova, Y.X. Liu, M.D. McGehee, J.M.J. Frechet, Journal of the American Chemical Society 126 (31) (2004) 9486.
[38] F.C. Krebs, M. Bjerring, J.S. Nielsen, N.C. Nielsen, Macromolecules 40 (16) (2007) 6012.
[39] K.C. Ho, H.Y. Wei, J.H. Huang, C.W. Chu, Acs Applied Materials & Interfaces 2 (5) (2010) 1281.
[40] F.C. Krebs, M. Jorgensen, K. Norrman, O. Hagemann, J. Alstrup, T.D. Nielsen, J. Fyenbo, K. Larsen, J. Kristensen, Solar Energy Materials and Solar Cells 93 (4) (2009) 422.
[41] K.P. Gritsenko, A.M. Krasovsky, Chemical Reviews 103 (9) (2003) 3607.
[42] M. Angelopoulos, G.E. Asturias, S.P. Ermer, A. Ray, E.M. Scherr, A.G. Macdiarmid, M. Akhtar, Z. Kiss, A.J. Epstein, Molecular Crystals and Liquid Crystals 160 (1988) 151.
[43] A. Biswas, Z. Marton, J. Kanzow, J. Kruse, V. Zaporojtchenko, F. Faupel, T. Strunskus, Nano Letters 3 (1) (2003) 69.
[44] A. Biswas, O.C. Aktas, J. Kanzow, U. Saeed, T. Strunskus, V. Zaporojtchenko, F. Faupel, Materials Letters 58 (9) (2004) 1530.
[45] F. Faupel, H. Takele, H. Greve, C. Pochstein, V. Zaporojtchenko, Nanotechnology 17 (14) (2006) 3499.
[46] F. Faupel, H.T. Beyene, V.S.K. Chakravadhanula, C. Hanisch, M. Elbahri, T. Strunskus, V. Zaporojtchenko, L. Kienle, Journal of Materials Science 45 (21) (2010) 5865.
[47] C. Vree, S.G. Mayr, Journal of Applied Physics 104 (8) (2008).
[48] M. Irimia-Vladu, N. Marjanovic, A. Vlad, A.M. Ramil, G. Hernandez-Sosa, R. Schwodiauer, S. Bauer, N.S. Sariciftci, Advanced Materials 20 (20) (2008) 3887.
[49] H.Y. Wei, L. Scudiero, H. Eilers, Applied Surface Science 255 (20) (2009) 8593.
[50] P. Kovacik, G. Sforazzini, A.G. Cook, S.M. Willis, P.S. Grant, H.E. Assender, A.A.R. Watt, Acs Applied Materials & Interfaces 3 (1) (2011) 11.
[51] Z. Mo, K.B. Lee, Y.B. Moon, M. Kobayashi, A.J. Heeger, F. Wudl, Macromolecules 18 (10) (1985) 1972.
[52] S.A. Chen, J.M. Ni, Macromolecules 25 (23) (1992) 6081.
[53] M. Sankir, Z. Kucukyavuz, S. Kucukyavuz, Journal of Applied Polymer Science 87 (13) (2003) 2113.
[54] S.Y. Sun, T. Salim, L.H. Wong, Y.L. Foo, F. Boey, Y.M. Lam, Journal of Materials Chemistry 21 (2) (2011) 377.
[55] Y. Furukawa, M. Akimoto, I. Harada, Synthetic Metals 18 (1–3) (1987) 151.
[56] M. Akimoto, Y. Furukawa, H. Takeuchi, I. Harada, Y. Soma, M. Soma, Synthetic Metals 15 (4) (1986) 353.
[57] G. Poussigue, C. Benoit, Journal of Physics-Condensed Matter 1 (48) (1989) 9547.
[58] F. Garnier, G. Tourillon, J.Y. Barraud, H. Dexpert, Journal of Materials Science 20 (8) (1985) 2687.
[59] P. Hermet, J.L. Bantignies, R. Almairac, J.L. Sauvajol, F. Serein, J.P. Lere-Porte, Journal of Physical Chemistry B 112 (40) (2008) 12662.
[60] S. Bruckner, W. Porzio, Makromolekulare Chemie-Macromolecular Chemistry and Physics 189 (4) (1988) 961.
[61] L.E. Alexander, X-Ray Diffraction Methods in Polymer Science, John Wiley & Sons Inc., 1969.
[62] C. Goh, R.J. Kline, M.D. McGehee, E.N. Kadnikova, J.M.J. Frechet, Applied Physics Letters 86 (12) (2005).
[63] V.D. Mihailetchi, H.X. Xie, B. de Boer, L.J.A. Koster, P.W.M. Blom, Advanced Functional Materials 16 (5) (2006) 699.
[64] G. Garcia-Belmonte, A. Munar, E.M. Barea, J. Bisquert, I. Ugarte, R. Pacios, Organic Electronics 9 (5) (2008) 847.
[65] A.L. Ayzner, C.J. Tassone, S.H. Tolbert, B.J. Schwartz, Journal of Physical Chemistry C 113 (46) (2009) 20050.
[66] D. Chen, F. Liu, C. Wang, A. Nakahara, T.P. Russell, Nano Letters 11 (5) (2011) 2071.
[67] J.S. Moon, C.J. Takacs, Y.M. Sun, A.J. Heeger, Nano Letters 11 (3) (2011) 1036.
[68] K.H. Lee, P.E. Schwenn, A.R.G. Smith, H. Cavaye, P.E. Shaw, M. James, K.B. Krueger, I.R. Gentle, P. Meredith, P.L. Burn, Advanced Materials 23 (6) (2011) 766.
[69] J.S. Kim, Y. Park, D.Y. Lee, J.H. Lee, J.H. Park, J.K. Kim, K. Cho, Advanced Functional Materials 20 (4) (2010) 540.
[70] P.E. Shaw, A. Ruseckas, I.D.W. Samuel, Advanced Materials 20 (18) (2008) 3516.
[71] U. Salzner, J.B. Lagowski, P.G. Pickup, R.A. Poirier, Synthetic Metals 96 (3) (1998) 177.
[72] A. Geiser, B. Fan, H. Benmansour, F. Castro, J. Heier, B. Keller, K.E. Mayerhofer, F. Nuesch, R. Hany, Solar Energy Materials and Solar Cells 92 (4) (2008) 464.